

Novel features extraction: pigment epithelial detachment detection using machine learning algorithms

Sheeba Thankappan Mercy¹, Albert Antony Raj Saminathan¹, Anand Murugadhas²,
Anshy Princella Anand Sheeba³

¹Department of Computer Applications, Faculty of Science and Humanities, SRM Institute of Science and Technology, Kattankulathur, India

²Department of Networking and Communications, SRM Institute of Science and Technology, Kattankulathur, India

³Department of Electronics and Communication Engineering, SRM Institute of Science and Technology, Kattankulathur, India

Article Info

Article history:

Received Mar 18, 2024

Revised Oct 1, 2024

Accepted Oct 23, 2024

Keywords:

Artificial neural network

Machine learning

Optical coherence tomography

Pigment epithelial detachment

Pigment epithelium layer

ABSTRACT

The majority of the retinal diseases have visual symptoms. Any area of the retina, a delicate layer of tissue on the interior the posterior wall of the human eye, can be impacted by retinal disorders. Optical coherence tomography (OCT) is the utmost commonly used imaging procedure for diagnosing retinal disorders such as age-related macular degeneration (ARMD), diabetic retinopathy, pigment epithelial detachment (PED), macular holes, and more. In this study, we put forth a brand-new technique for accurately extracting features from OCT images to identify PED diseases. For the preprocessing step, we examined the wiener filtering method. After that, we segmented the retinal pigment epithelium (RPE) layer used to the thresholding method, extracted the features from the RPE layer, and then gave the features to machine learning (ML) classifiers like the support vector machine (SVM), logistic regression (LR), k-nearest neighbors (KNN), decision tree (DT), random forest (RF), naive Bayes (NB), and artificial neural network (ANN). The total dataset about 200 images among 100 is normal and 100 is PED, we trained the dataset as an unbalanced and balanced group. The RF is the best outcome in comparison of other classifiers. The overall outcome of random forest is 100% accuracy.

This is an open access article under the [CC BY-SA](https://creativecommons.org/licenses/by-sa/4.0/) license.



Corresponding Author:

Anand Murugadhas

Department of Networking and Communications, SRM Institute of Science and Technology

Kattankulathur - 603203, Tamil Nadu, India

Email: anandm3@srmist.edu.in

1. INTRODUCTION

A specialized sense organ called the human eye is able to take in visual images, which are subsequently transmitted to the brain. It has a sphere-like shape and responds to light to give humans the ability to see. The behind segment of the visual organ is put up of the vitreous body, retina, choroid, and sclera, while the foremost segment of the eye is put up of the cornea, iris, and lens. Just between the iris and pupil, there is a lens that supports brighten the posterior plane of the eye. The major of the visual organ is occupied with the vitreous, a translucent gel [1]. Eye pupil and lens let thin-light to reach the inner eye surface. The inner eye surface is a layer of unique light-sensing cells that covers the inside of the eye. It converts light into electrical impulse. These impulses travel from the retina to the brain by the optic-nerve. The macula, a tiny, particularly sensitive area of the retina, is responsible for the center vision. The type and amount of pigment found in the iris defines the color of the eyes. A person's eye color is determined by how many genes they receive from each parent [2]. Figure 1 depicts the human eye anatomy. Every day, retinal

anomalies are diagnosed in thousands of people. Using optical coherence tomography (OCT) scan images, qualified medical personnel must inspect and categorize retinal abnormalities as part of the diagnosing procedure. In general, this is a drawn-out manual process. The detection and classification of medical images using machine intelligence is now more practical because to recent developments in computer vision. Alternative solutions to this issue, such as the creation of an automated program that might help medical personnel in the detection and categorization process earlier, could be found.

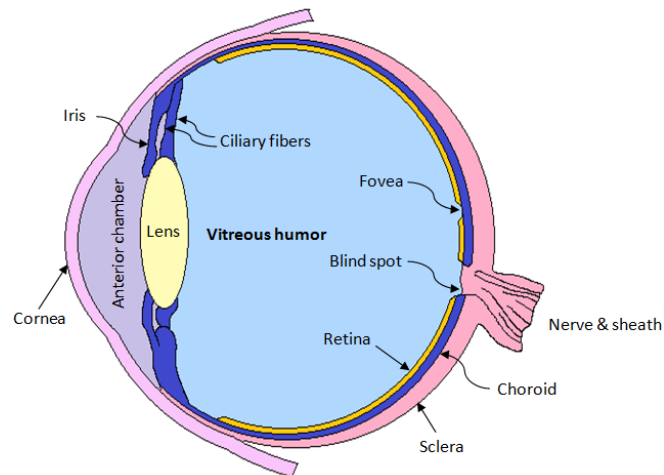


Figure 1. Human eye

Using OCT, is a simple scanning approach that generates heightened clarity images a cross-section in retina images, physicians can collect valuable information for identifying many retinal diseases. Despite its advantages, manual OCT image analysis needs extensive time and is greatly reliant on the analyst's personal Proficiency. The study [3] focuses on the clinical interpretation of retinal disorders using machine learning to examine OCT images. The sample OCT image is shown in Figure 2. There are 11 layers in the human eye. Figure 3 shows the retinal layers in the human retinal OCT images. The layers include: inner photo receptor layer, inner nuclear layer, inner plexiform layer, choroid, outer nuclear layer, outer plexiform layer, retinal pigment epithelium layer, and external limiting membrane.

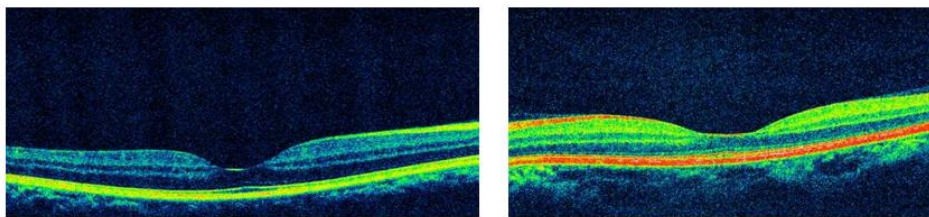


Figure 2. Normal OCT images

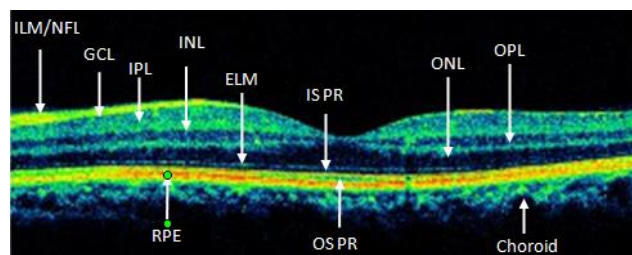


Figure 3. Retinal layers

Age-related macular degeneration (AMD), the mostly frequent eye disease process, is characterized by a frequent characteristic called retinal pigment epithelial detachment (PED) [4]. Initial research was restricted to evaluating these PEDs using planar imaging techniques such fluorescein angiography and color fundus photography. The visual system offers a unique window into the ageing process and the challenges associated with developing effective treatments for age-related eye illnesses. This article suggests a number of potential ML techniques to tackle these issues. Retinal image screening was employed as an example application-domain to serve as the investigation's focal point and to assess the provided theories [5]. More specifically, AMD was detected by classifying images as AMD normal/abnormal illness. Figure 4 shows the PED images. The retina is the inner layer of the eye from which light signals are transformed into neurological signals. Since it contains a variety of rod and cone pigments, it is certain to dull light and affect color perception. There are several layers of sanitary and physiological concern in the retina. Generally speaking, damage to specific layers causes various abnormalities as well as visual loss. For the diagnosis of several retinal illnesses, including central-serous-retinopathy, diabetic-retinopathy, macular-edema, macular-hole, chronic glaucoma, and blindness, OCT remains a crucial tool. Xiang *et al.* [6] introduced the fluid segmentation technique for OCT retinal images. Xiang *et al.* [7] deployed a supervised machine learning strategy to suggest segmenting layers and neovascularization using OCT images. In study [8], to organize subretinal fluid (SRF) and PED aspects among OCT images. In study [9], optical coherence tomography (OCT) images can be utilized to recognize the macular hole described by Mendes *et al.* through the upper borders of the internal limiting membrane (ILM) and the retinal pigment epithelium (RPE). Azamen *et al.* [10] suggested employing machine learning algorithms based on risk variables to forecast the onset of diabetic retinopathy.

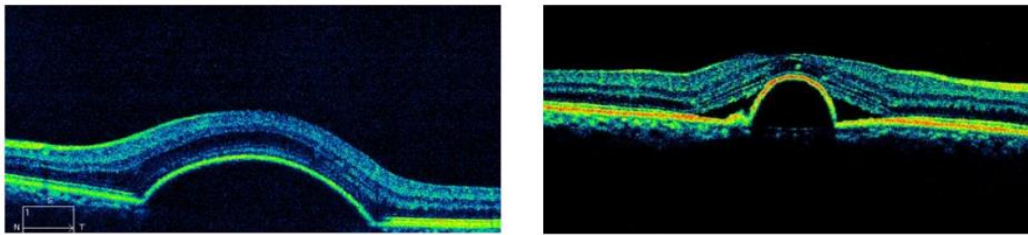


Figure 4. Sample PED images

2. LITERATURE REVIEW

A separating of the RPE from the inside collagenic layer of Bruch-membrane is assigned to as retinal pigment epithelial detachment (PED). Both the dry and wet forms of age-related -macular-degeneration frequently exhibit this symptom. To be able to aid in the identifying and managing of this significant aspect of age-related macular degeneration (ARMD), this examination purposes to give a thorough overview of the pathology, medical and imaging aspects, normal flow and therapy of the several forms of PED [11]–[13]. Koh *et al.* [14] employed 404 normal and 1,082 pathological fundus retinal pictures to classify regular from irregular visuals using a random forest (RF) classifier. Without segmenting, energy and entropy information were extracted using the 2D continuous wavelet transform, which produced great accuracy and allowed the classification of three distinct groups of fundus images. In order to identify photos with and without fat deposits, support vector machine (SVM), k-nearest neighbors (KNN), and machine learning (ML) classification were examined, which produced greater accuracy and sensitivity [14]. The three feature extraction techniques were compared, and in adding to differentiating characteristics, hidden Markov model (HMM) and SVM classifiers were employed to determine whether the indicator was Parkinson's-related or not [15]. Medical image compression is accomplished using random permutation coefficient-based compressed sensing (CS). With this technique, a high-quality flattened image is maintained with a respectable amount of the restored image [16]. The amplitude modulation-frequency modulation (AM-FM) technology is used to analyze textures in segmented images. Each image sample's current amplitude and frequency data are gathered and quantified. To assess if the artery is normal or aberrant, it is then associated to a typical material model [17]. ML system written in MATLAB was used to identify AMD created on fundus retinal pictures from the FRI database. Compared to other ML classifiers, the SVM has a classification accuracy that is higher (>93%) [18]. Layer extraction of OCT images has been advanced through a variety of techniques, with the graph search algorithm serving as the cornerstone in many approaches [19]–[26]. Recently, Tian *et al.* [27] suggested a shortest-path dependent graph-search to deduct

retinal borders by seeking the shortest-path between two end-nodes, using the graph search algorithm with Dijkstra's algorithm. The search region's restriction and downsampling helped to lower the time complexity. SVM with characteristics dependent on picture intensities and gradients were utilized by Vermeer *et al.* [28] to identify five retinal interfaces. In order to determine the initial surfaces, Srinivasan *et al.* [29] coupled SVM with the average-intensity of every row. Since the difference among adjacent surfaces in normal eyes was significantly larger than in OCT pictures of damaged retinas, the characteristics were primarily created for edge classification of ordinary eyes. The segmentation of retinal anomalies was the focus of many more techniques [30]. An automated technique for symptomatic-exudate-associated derangements (SEAD) footmark deduction was described by Quellec *et al.* [31]. The top and bottom layers of the OCT were segmented using a graph cut method, the subretinal fluid and sub-RPE fluid among the surfaces were segmented using a split Bregman-based segmentation method [32]. Finally, the actual fluid regions were segmented using a random forest classifier that had been developed. Diabetes-related macular edema was segmented by Wang *et al.* [33] using a fuzzy-level set-dependent segment technique.

3. METHOD

PED and normal images may be found in the OCT image database, which will make classifying it more effective and precise. OCT scans from normal retina and PED can have different levels of illness; a professional or ML expert is needed to help the practitioner classify the findings. Figure 5 depicts the suggested methodology. Preprocessing, dataset, training and classification make up the technique part. The color image was changed to a grayscale version for analysis, and the pixel values were expanded to cover the whole range between 0 and 1. The creation of a macular hole is then determined using the suggested methods after processing this normalized image. The normalized image is exposed to the median filter to decrease noise, producing the filtering image [34]. In the preprocessing we used two steps. The first step denoising and the second step RPE layer segmentation.

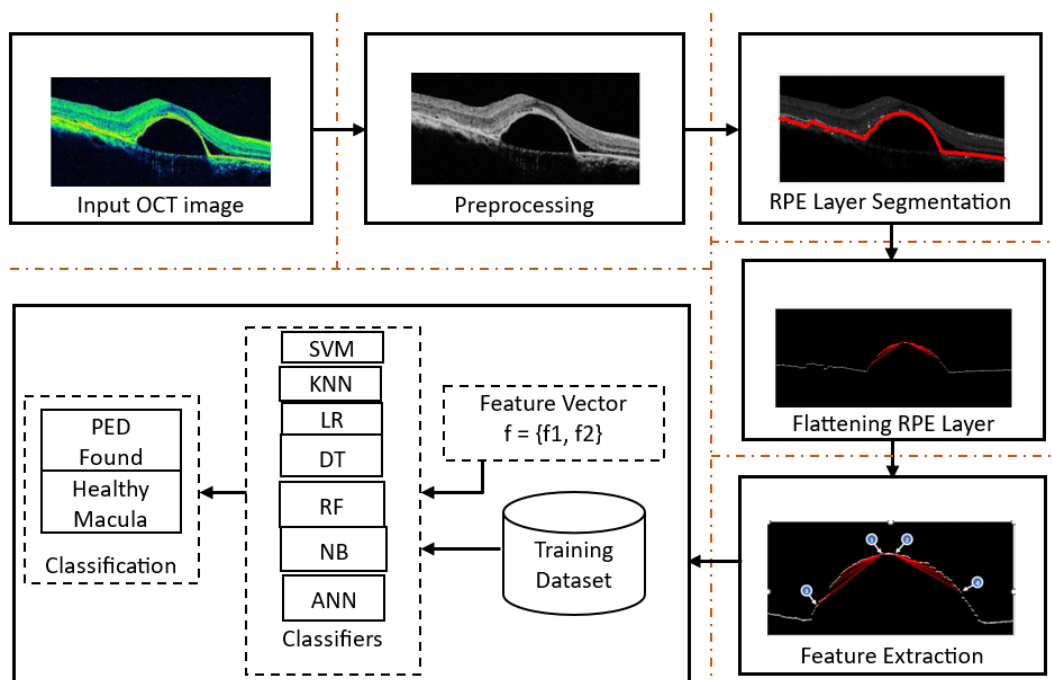


Figure 5. Proposed methodology

3.1. Denoising

Speckle noise is commonly observed in OCT images, degrading their quality significantly. To mitigate this issue, we employed a Wiener filtering technique to remove speckle noise and convert the original image into grayscale. Figure 6 shows the outcome of the image pre-processing with original image in Figure 6(a), grayscale image in Figure 6(b) and denoised image in Figure 6(c). We analyzed the various types of filtering technique such as mean, median, gaussian, bilateral and wiener. Based on the metrics such as MSE, PSNR and PSR wiener filter is the accurate decrease the speckle noise [35].

3.2. RPE layer segmentation

In the second step of preprocessing, we perform RPE-layer segmentation. For this segmentation, we utilize the thresholding method. The RPE layer exhibits uniform brightness and smoothness, allowing us to analyze each pixel value along the column. Figure 7 shows the output of the RPE layer segmentation with RPE layer on healthy grayscale image in Figure 7(a), RPE overlay on the original healthy image in Figure 7(b), RPE-layer with PED on a grayscale image in Figure 7(c) and RPE layer on PED-image in Figure 7(d). We analyzed the RPE layer segmentation with 20 images of healthy and 20 images of PED images and got healthy macula fully detected correctly and PED 19 images detected correctly. One key approach in image segmentation is thresholding. This method may be described as (1),

$$T = T[x, y, p(x, y), f(x, y)] \quad (1)$$

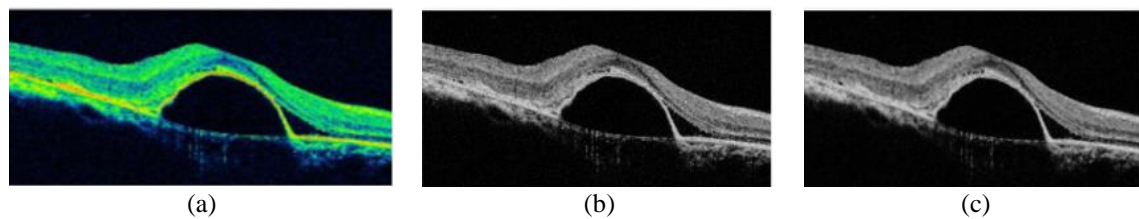


Figure 6. Preprocessing: (a) original image, (b) gray-scale image, and (c) denoised image (wiener filter)

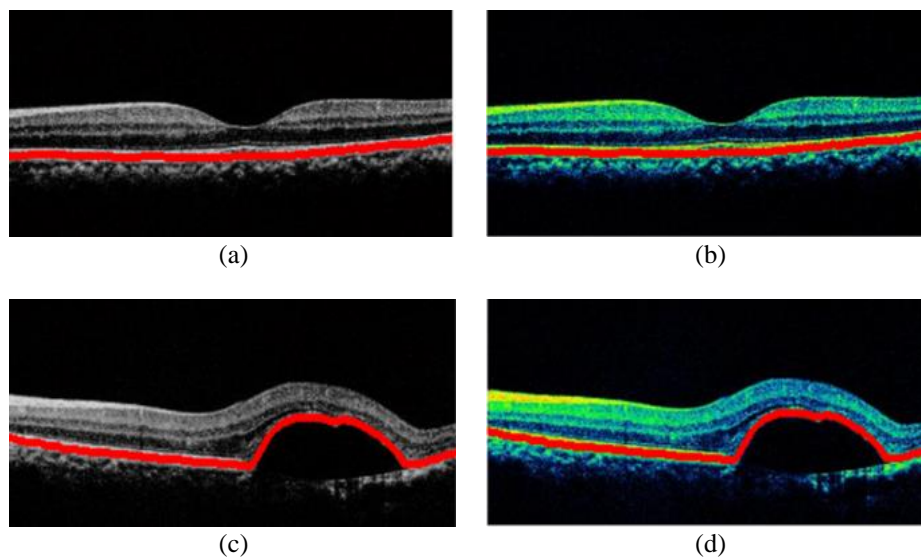


Figure 7. Layer segmentation: (a) RPE layer on healthy grayscale image, (b) RPE overlay on the original healthy image, (c) RPE-layer with PED on a grayscale image (d) RPE layer on PED-image

3.3. Extract the features

The process of feature extraction is crucial for recognizing the macular-hole in the OCT image. Feature extraction process involves two parts. The list of border pixels for each column is only used to choose one pixel from each column in the first step. The 2nd step identifies the 2 largest y-axis differences between 2 successive pel [36]–[38]. The characteristics of images have long been manually retrieved using various feature-engineering techniques in classic machine learning methods. The art of extract significant and valuable pattern from data that necked eyes cannot see is known as feature engineering. Machine learning models can identify between classes more easily by extracting features. Because it reduces the amount of labels that must be considered for precise classification, this characteristic is beneficial for machine learning algorithms. Therefore, feature engineering is the most crucial ability for achieving good results for the majority of prediction tasks [39]. Traditional image classification and prediction techniques include machine learning classifiers and regressors like KNN, SVM, and artificial neural network (ANN). Color, edges, form,

texture, local binary patterns (LBP), and histograms of the oriented gradients (HOG) are further hand-drawn picture characteristics. After the features have been recovered, a classifier is trained to carry out the classification, detection, or prediction job for the images [2]. In this work to detected the PED, we analyzed machine learning classifications are decision tree (DT), logistic regression (LR), naive Bayes (NB), ANN, RF, SVM and KNN. To predicted the PED we used four features are extracted such as *Max_Left_Height* (M_L_H), *Number_of_Left_Down_Points* (N_L_D_P), *No_of_Right_Down_Points* (N_R_D_P) and *Max_Right_Height* (M_R_H). These features are significantly predicted the PED disease and Figure 8 depicts the outcome of the feature extraction with PED image with RPE-layer in Figure 8(a), separated RPE-layer in Figure 8(b) and extracted four features in Figure 8(c).

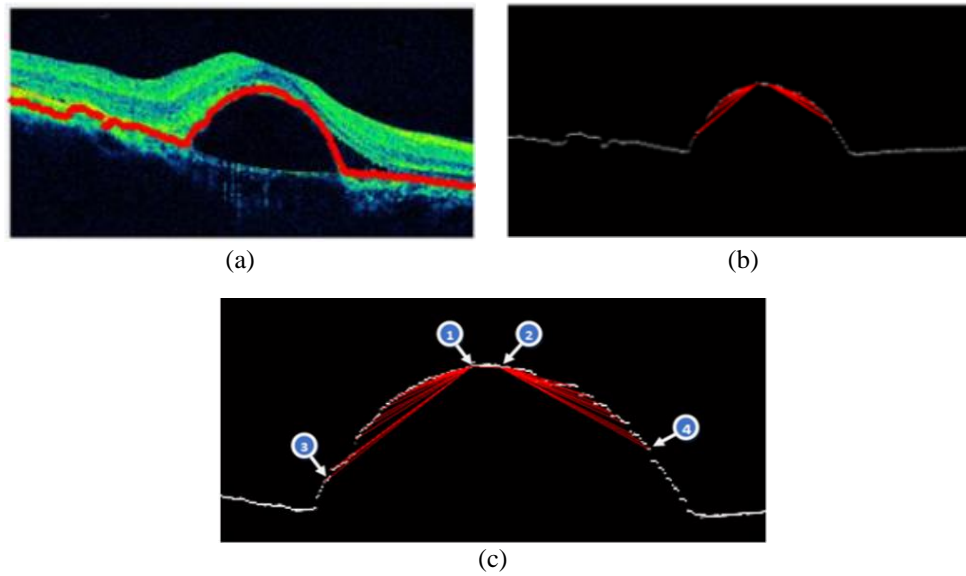


Figure 8. Feature extraction: (a) PED image with RPE-layer, (b) separated RPE-layer, and (c) extracted four features

Here, we used (2)-(4) to find out the top-layer, bottom-layer and max-height:

$$tp = \min(L_i) \quad (2)$$

$$btm = \max(L_i) \quad (3)$$

$$mHeight = btm - tp \quad (4)$$

where L_i is the RPE layer's y axis value for each x axis value, where x extends from zero to the width of the image. Because the top-left corner of the image is at (0, 0), the 'min' method is used to get the smallest y-axis value of the RPE layer, in order to obtain the top of the layer. The bottommost layer is identified using the 'max' function. The top-left point is then determined by repeating the line from zero to the line's highest point. Iterating from the estimated top-left point to the line's highest point yields the top-right point. The top-left point is then used to extract 20 points to build a bounding rectangle. The RPE layer height governs the width of the rectangle.

$$w = mHeight \quad (5)$$

In this study, we extracted 20 points from the top-left corner and 20 points from the top-right corner to governs the curve. The interval is calculated for the 20 points extracted from the top-left corner as (6):

$$d = \frac{w}{20} \quad (6)$$

The line height of each point is then obtained by iterating the line points 20 times backward from the top-left point:

$$lPoints_i = mHeight - (L_{(topLeftPoint-d*i)}) \quad (7)$$

where i differs from 1 to 20.

The subsequent equation extracted the top-right 20 points:

$$rPoints_i = mHeight - (L_{(topRightPoint+d*i)}) \quad (8)$$

where i varies from 1 to 20.

The equations (9) and (10) are used to extract the maximum left height (M_L_H) and maximum right height (M_R_H) features:

$$M_L_H = \max(lPoints_i) \quad (9)$$

$$M_R_H = \max(rPoints_i) \quad (10)$$

By comparing the subsequent left-points, the number of left down points (N_L_D_P) characteristic is then computed. Increase the counter N_L_D_P if a left-point value is smaller than the following left-point value. By comparing the right-points and increasing the counter, the number of right down points (N_R_D_P) feature is determined. The algorithm to detect the four distinct features to detect PED is given in the Algorithm 1.

$$N_L_D_P = N_L_D_P + 1 \text{ if } (lPoints_i < lPoints_{(i+1)}) \quad (11)$$

$$N_R_D_P = N_R_D_P + 1 \text{ if } (rPoints_i < rPoints_{(i+1)}) \quad (12)$$

Algorithm 1. Extract_Features (L)

INPUT:

L - An array contains y values of each column pixel of the layer

OUTPUT:

maxLeftHeight - Maximum left height

maxRightHeight - Maximum right height

noOfLeftDownPoints - Number of left down points

noOfRightDownPoints - Number of right down points

Step-1: $t = \min(L)$

Step-2: $btm = \max(L)$

Step-3: $lHeight_i = btm - L_i$;

Step-4: $mHeight = btm - t$;

Step-5: Repeat Step-6 for $i = 1$ to $\text{length}(L)$

Step-6: if $(lHeight_i = mHeight)$ goto Step-7

Step-7: $tpLPoint = i$

Step-8: $w = \maxHeight$

Step-9: $noOfPoints = 20$

Step-10: $distance = w/noOfPoints$;

Step-11: $lPoints(1) = mHeight$;

Step-12: Repeat Step-13 and Step-14 for $j = 1$ to $noOfPoints$

Step-13: $pos = tpLPoint - d_BtwPoints * j$;

Step-14: $lPoints(j + 1) = lHeight(pos)$;

Step-15: Repeat Step-16 for $j = i$ to $l(lHeight)$

Step-16: if $(lHeight(j) \neq mHeight)$ goto Step-17

Step-17: $tRightPoint = j$;

Step-18: $rPoints(1) = mHeight$;

Step-19: Repeat Step-20 and Step-21 for $k = 1$ to $noOfPoints$

Step-20: $pos = topRightPoint + distanceBtwPoints * k$

Step-21: $rightPoints(k + 1) = lineHeight(pos)$

Step-22: $maxLHeight = \max(leftHeight)$;

Step-23: $maxRightHeight = \max(rightHeight)$;

Step-24: $noOfLeftDownPoints = 0$;

Step-25: $noOfRightDownPoints = 0$;

Step-26: Repeat Step-27 to Step-30 for $i = 2$ to $noOfPoints$

Step-27: if $((leftHeight_i - leftHeight_{i-1}) > 0)$

Step-28: $noOfLeftDownPoints = noOfLeftDownPoints + 1$;

Step-29: if $((rHeight_i - rHeight_{i-1}) > 0)$

Step-30: $noOfRightDownPoints = noOfRightDownPoints + 1$;

Step-31: Stop

4. RESULTS AND DISCUSSION

The original OCT images were converted into grayscale, and then we applied the Wiener filtering technique to effectively remove speckle noise, then extracted the RPE layer used to threshold method, while PED found in the RPE layer, then to detected the PED. We extracted four features were to identified PED with machine learning classifiers. Toal 200 images among 100 images of normal retina, 100 images of PED, a local dataset. Retinal OCT images with normal and PED retinas are included in the testing dataset along with a training dataset. In this work ordinary retinal images are assigned a value of 0, whereas PED retinal image is assigned a value of 1. Based on the Table 1, analyzed the true-positive (T-P), false-negative (F-N), true-negative (T-N) and false-positive (F-P) parameters and Figure 9 depicts the graphical representation of these parameters.

Based on the Table 2, to calculate the following metrics are accuracy, sensitivity, specificity, precision and F1-score and Figure 10 shows the graphical representation of these metrics. The confusion matrix may be used to determine the accuracy, sensitivity, specificity and precision. Figure 11 depicts the confusion matrix for the SVM model. Based on the Figure 10, the random forest (RF) model is performed the best classification model comparing the other classifiers. RF was provided for 100% accuracy, 100% sensitivity, 100% specificity, 100% precision, and 100% F1-score. The area under the ROC curve (AUC) of receiver operating characteristics (ROC) curve will be used to link the performance of the ML classifier with binary classification. The RF-ML model's AUC was 1.0. The RF-ML classifier model suggested that global achievement is superior in classifying among PED and ordinary retina of OCT-images because the AUC value is to 1 (high), as shown in Figure 12.

Table 1. Result of the machine learning classifications and ANN

Classifiers	T-P	F-N	T-N	F-P
SVM	20	0	18	2
KNN	18	2	18	2
LR	20	0	19	1
DT	20	0	18	2
RF	20	0	20	0
NB	20	0	18	2
BPNN	20	0	18	2

Note: BPNN - backpropagation neural network

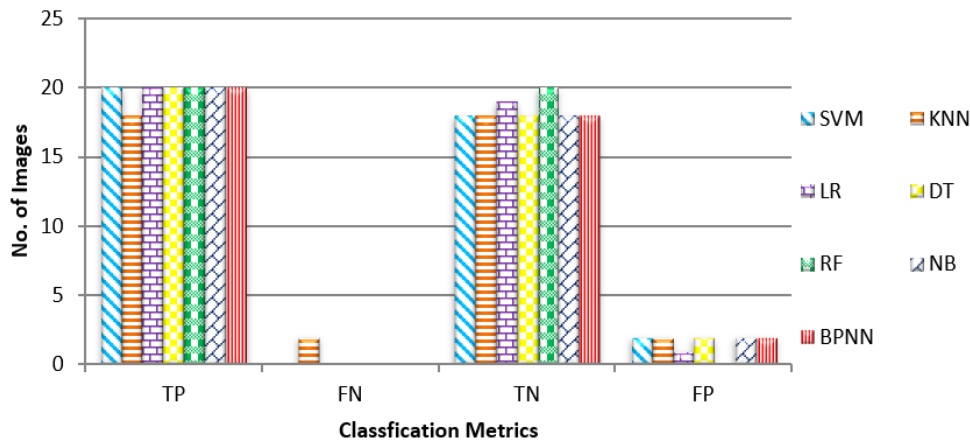


Figure 9. Analysis of classifiers using T-P, F-N, T-N and F-P

Table 2. Analysis report of machine learning classifiers and BPNN

ML-classifiers	Accuracy	Sensitivity	Specificity	Precision	F1-score
SVM	0.95	1.00	0.9	0.9091	0.9524
KNN	0.9	0.90	0.9	0.9	0.9
LR	0.975	1.00	0.95	0.9524	0.9756
DT	0.95	1.00	0.9	0.9091	0.9524
RF	1.00	1.00	1.00	1.00	1.00
NB	0.95	1.00	0.90	0.91	0.9524
BPNN	0.95	1.00	0.90	0.91	0.9524

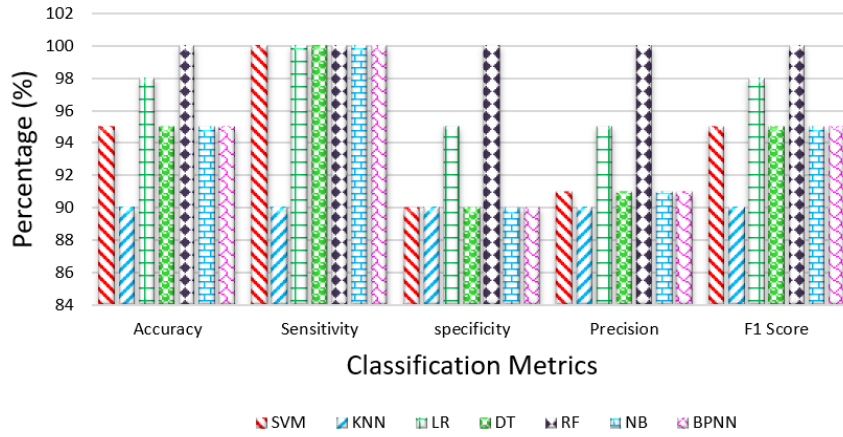


Figure 10. Analysis of metrics of machine learning classifiers and BPNN

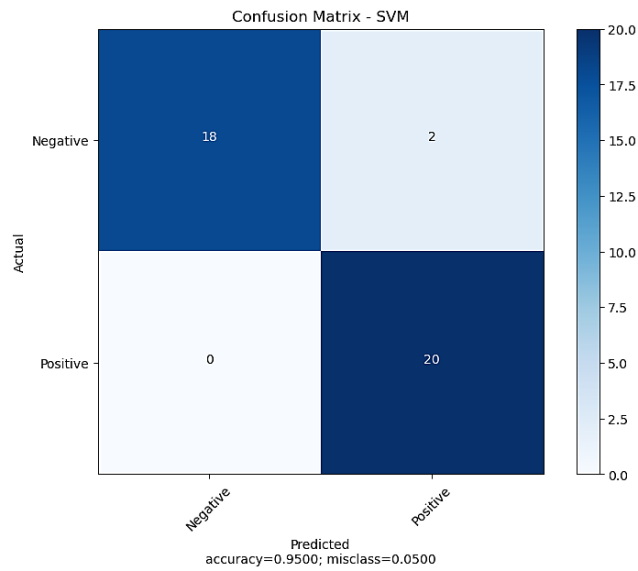


Figure 11. Confusion matrix of SVM

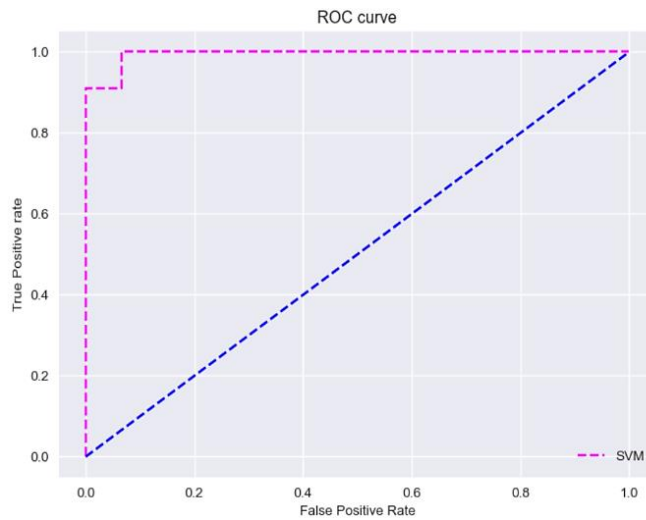


Figure 12. ROC curve for SVM and AUC for 0.9878787878787879

5. CONCLUSION

The primary contribution of this work is, the extraction of features from OCT PED images. In OCT, which consists of PED and normal retina, may be detected PED using machine learning based classifier models and back propagation neural network. To assess classification parameters including accuracy, sensitivity, specificity, precision, and F1-score, various machine learning classifier models were utilized. The SVM-accuracy, SVM-sensitivity, SVM-specificity, SVM-precision and SVM-F1-score of SVM is 95%, 100%, 90%, 90% and 95%, KNN is 90%, 90%, 90%, 90% and 90%, LR is 97%, 100%, 95%, 95% and 97%, DT is 95%, 100%, 90%, 90% and 95%, RF is 100%, 100%, 100%, 100% and 100%, NB is 95%, 100%, 90%, 91% and 95% and ANN is 95%, 100%, 90%, 91% and 95%. The LR ROC curve had an AUC of 0.9939, while the DT was 0.9333, the SVM was 0.987878, the KNN's was 0.94848484848486, and the NB was 0.99393, while the RF was 1.0. The RF performed as the best classifier to detected the PED based on the aforementioned results for the classification of ML. In the categorization of ML normal and PED, KNN performs the poorest. The findings of the machine learning-based models' random forest, decision tree, logistic regression, support vector machine, and naive Bayes developed by classifying metrics using the proper technique were efficient and practical in detected normal retinal and PED in OCT images. Finally, in terms of PED identification in OCT images, the random forest classifier gives best performance among the others. In future we will identify another disease.




REFERENCES

- [1] B. K. Triwijoyo, B. S. Sabarguna, W. Budiharto, and E. Abdurachman, "Deep learning approach for classification of eye diseases based on color fundus images," in *Diabetes and Fundus OCT*, Elsevier, 2020, pp. 25–57, doi: 10.1016/b978-0-12-817440-1.00002-4.
- [2] U. Fatema, J. Hasan, and S. A. H., "Classification performance analysis of retinal OCT image using handcrafted and deep learning feature with support vector machine," B.S. thesis, Department of Electrical and Electronic Engineering, Hajee Mohammad Danesh Science and Technology University, 2021.
- [3] P. K. Karn and W. H. Abdulla, "On machine learning in clinical interpretation of retinal diseases using OCT images," *Bioengineering*, vol. 10, no. 4, Mar. 2023, doi: 10.3390/bioengineering10040407.
- [4] S. Zayit-Soudry, I. Moroz, and A. Loewenstein, "Retinal pigment epithelial detachment," *Survey of Ophthalmology*, vol. 52, no. 3, pp. 227–243, May 2007, doi: 10.1016/j.survophthal.2007.02.008.
- [5] S. Latha, R. Loganathan, and K. Shanmugam, "Machine learning classification of normal vs. age-related macular degeneration OCT images," *BOHR International Journal of Smart Computing and Information Technology*, vol. 2, no. 1, pp. 34–38, 2021, doi: 10.54646/bijscit.2021.16.
- [6] D. Xiang *et al.*, "Automatic retinal layer segmentation of OCT images with central serous retinopathy," *IEEE Journal of Biomedical and Health Informatics*, vol. 23, no. 1, pp. 283–295, Jan. 2019, doi: 10.1109/jbhi.2018.2803063.
- [7] D. Xiang *et al.*, "Automatic segmentation of retinal layer in OCT images with choroidal neovascularization," *IEEE Transactions on Image Processing*, vol. 27, no. 12, pp. 5880–5891, Dec. 2018, doi: 10.1109/tip.2018.2860255.
- [8] Y. Huang and J. Hu, "Residual neural network-based classification of macular edema in OCT," in *2019 IEEE 31st International Conference on Tools with Artificial Intelligence (ICTAI)*, Nov. 2019, pp. 736–743, doi: 10.1109/ictai.2019.00107.
- [9] O. L. C. Mendes *et al.*, "Automatic segmentation of macular holes in optical coherence tomography images," *IEEE Access*, vol. 9, pp. 96487–96500, 2021, doi: 10.1109/access.2021.3092301.
- [10] N. T. N. N. Azamen, A. M. Ali, and N. A. A. Aziz, "Prediction of diabetic retinopathy based on risk factors using machine learning algorithms," in *2023 4th International Conference on Artificial Intelligence and Data Sciences (AiDAS)*, Sep. 2023, pp. 308–312, doi: 10.1109/aidas60501.2023.10284646.
- [11] M. Karampelas, P. Malamos, P. Petrou, I. Georgalas, D. Papaconstantinou, and D. Brouzas, "Retinal pigment epithelial detachment in age-related macular degeneration," *Ophthalmology and Therapy*, vol. 9, no. 4, pp. 739–756, Aug. 2020, doi: 10.1007/s40123-020-00291-5.
- [12] A. García-Floriano, Á. Ferreira-Santiago, O. Camacho-Nieto, and C. Yáñez-Márquez, "A machine learning approach to medical image classification: Detecting age-related macular degeneration in fundus images," *Computers & Electrical Engineering*, vol. 75, pp. 218–229, May 2019, doi: 10.1016/j.compeleceng.2017.11.008.
- [13] S. Latha, D. Samiappan, and R. Kumar, "Carotid artery ultrasound image analysis: A review of the literature," *Proceedings of the Institution of Mechanical Engineers, Part H: Journal of Engineering in Medicine*, vol. 234, no. 5, pp. 417–443, Jan. 2020, doi: 10.1177/0954411919900720.
- [14] J. E. W. Koh *et al.*, "Diagnosis of retinal health in digital fundus images using continuous wavelet transform (CWT) and entropies," *Computers in Biology and Medicine*, vol. 84, pp. 89–97, May 2017, doi: 10.1016/j.combiomed.2017.03.008.
- [15] H. Kuresan, D. Samiappan, and S. Masunda, "Fusion of WPT and MFCC feature extraction in Parkinson's disease diagnosis," *Technology and Health Care*, vol. 27, no. 4, pp. 363–372, 2019, doi: 10.3233/THC-181306.
- [16] R. Monika, S. Dhanalakshmi, and S. Sreejith, "Coefficient random permutation-based compressed sensing for medical image compression," in *Advances in Electronics, Communication and Computing*, Springer Singapore, 2017, pp. 529–536, doi: 10.1007/978-981-10-4765-7_56.
- [17] D. Samiappan and V. Chakrapani, "Classification of ultrasound carotid artery images using texture features," *International Review on Computers and Software*, vol. 8, no. 4, pp. 933–940, 2013.
- [18] V. Rajinikanth *et al.*, "Automated classification of retinal images into AMD/non-AMD Class—a study using multi-threshold and Gaussian-filter enhanced images," *Evolutionary Intelligence*, vol. 14, no. 2, pp. 1163–1171, Mar. 2021, doi: 10.1007/s12065-021-00581-2.
- [19] M. K. Garvin, M. D. Abramoff, R. Kardon, S. R. Russell, X. Wu, and M. Sonka, "Intra-retinal layer segmentation of 3D optical coherence tomography using coarse grained diffusion map," *IEEE Transactions on Medical Imaging*, vol. 27, no. 10, pp. 1495–1505, Oct. 2008, doi: 10.1109/tmi.2008.923966.
- [20] M. K. Garvin, M. D. Abramoff, X. Wu, S. R. Russell, T. L. Burns, and M. Sonka, "Automated 3-D intraretinal layer segmentation of macular spectral-domain optical coherence tomography images," *IEEE Transactions on Medical Imaging*, vol. 28, no. 9,




- pp. 1436–1447, Sep. 2009, doi: 10.1109/tmi.2009.2016958.
- [21] S. Lu, C. Y. Cheung, J. Liu, J. H. Lim, C. K. Leung, and T. Y. Wong, “Automated layer segmentation of optical coherence tomography images,” *IEEE Transactions on Biomedical Engineering*, vol. 57, no. 10, pp. 2605–2608, Oct. 2010, doi: 10.1109/tbme.2010.2055057.
- [22] Q. Song, J. Bai, M. K. Garvin, M. Sonka, J. M. Buatti, and X. Wu, “Optimal multiple surface segmentation with shape and context priors,” *IEEE Transactions on Medical Imaging*, vol. 32, no. 2, pp. 376–386, Feb. 2013, doi: 10.1109/tmi.2012.2227120.
- [23] Q. Yang *et al.*, “Automated layer segmentation of macular OCT images using dual-scale gradient information,” *Optics Express*, vol. 18, no. 20, Sep. 2010, doi: 10.1364/oe.18.021293.
- [24] R. Kafieh, H. Rabbani, M. D. Abramoff, and M. Sonka, “Intra-retinal layer segmentation of 3D optical coherence tomography using coarse grained diffusion map,” *Medical Image Analysis*, vol. 17, no. 8, pp. 907–928, Dec. 2013, doi: 10.1016/j.media.2013.05.006.
- [25] G. Li, X. Chen, F. Shi, W. Zhu, J. Tian, and D. Xiang, “Automatic liver segmentation based on shape constraints and deformable graph cut in CT images,” *IEEE Transactions on Image Processing*, vol. 24, no. 12, pp. 5315–5329, Dec. 2015, doi: 10.1109/tip.2015.2481326.
- [26] D. Xiang *et al.*, “CorteXpert: a model-based method for automatic renal cortex segmentation,” *Medical Image Analysis*, vol. 42, pp. 257–273, Dec. 2017, doi: 10.1016/j.media.2017.06.010.
- [27] J. Tian, B. Varga, G. M. Somfai, W.-H. Lee, W. E. Smiddy, and D. Cabrera DeBuc, “Real-time automatic segmentation of optical coherence tomography volume data of the macular region,” *PLOS ONE*, vol. 10, no. 8, Aug. 2015, doi: 10.1371/journal.pone.0133908.
- [28] K. A. Vermeer, J. van der Schoot, H. G. Lemij, and J. F. de Boer, “Automated segmentation by pixel classification of retinal layers in ophthalmic OCT images,” *Biomedical Optics Express*, vol. 2, no. 6, May 2011, doi: 10.1364/boe.2.001743.
- [29] P. P. Srinivasan, S. J. Heflin, J. A. Izatt, V. Y. Arshavsky, and S. Farsiu, “Automatic segmentation of up to ten layer boundaries in SD-OCT images of the mouse retina with and without missing layers due to pathology,” *Biomedical Optics Express*, vol. 5, no. 2, Jan. 2014, doi: 10.1364/boe.5.000348.
- [30] J. Novosel, G. Thepass, H. G. Lemij, J. F. de Boer, K. A. Vermeer, and L. J. van Vliet, “Loosely coupled level sets for simultaneous 3D retinal layer segmentation in optical coherence tomography,” *Medical Image Analysis*, vol. 26, no. 1, pp. 146–158, Dec. 2015, doi: 10.1016/j.media.2015.08.008.
- [31] G. Quellec, K. Lee, M. Dolejsi, M. K. Garvin, M. D. Abramoff, and M. Sonka, “Three-dimensional analysis of retinal layer texture: Identification of fluid-filled regions in SD-OCT of the macula,” *IEEE Transactions on Medical Imaging*, vol. 29, no. 6, pp. 1321–1330, Jun. 2010, doi: 10.1109/tmi.2010.2047023.
- [32] W. Ding *et al.*, “Automatic detection of subretinal fluid and sub-retinal pigment epithelium fluid in optical coherence tomography images,” in *2013 35th Annual International Conference of the IEEE Engineering in Medicine and Biology Society (EMBC)*, Jul. 2013, pp. 7388–7391, doi: 10.1109/embc.2013.6611265.
- [33] J. Wang *et al.*, “Automated volumetric segmentation of retinal fluid on optical coherence tomography,” *Biomedical Optics Express*, vol. 7, no. 4, Mar. 2016, doi: 10.1364/boe.7.001577.
- [34] M. Anand and C. Jayakumari, “A new approach to detect macular hole from optical coherence tomography images,” *Indian Journal of Public Health Research and Development*, vol. 10, no. 7, p. 1235, 2019, doi: 10.5958/0976-5506.2019.01755.8.
- [35] T. M. Sheeba and S. A. A. Raj, “Analysis of noise removal techniques on retinal optical coherence tomography images,” *International Journal of Advanced Computer Science and Applications*, vol. 13, no. 9, 2022, doi: 10.14569/ijacsa.2022.0130948.
- [36] T. M. Sheeba and S. A. A. Raj, “Prediction of pigment epithelial detachment in optical coherence tomography images using machine learning,” *International Journal of Advanced Computer Science and Applications*, vol. 15, no. 4, 2024, doi: 10.14569/ijacsa.2024.0150456.
- [37] S. T. M. and A. A. R. S., “Distinct features for detection of pigment epithelial detachment using machine learning and artificial neural network in two-dimensional optical coherence tomography images,” *International Journal of Intelligent Systems and Applications in Engineering*, vol. 12, no. 14, pp. 338–347, 2024.
- [38] M. Anand and C. Jayakumari, “Automated detection of full thickness macular hole in optical coherence tomography images,” *Journal of International Pharmaceutical Research*, vol. 46, no. 4, pp. 45–49, 2019.
- [39] K. A. Tarnowska and A. Patel, “Log-based malicious activity detection using machine and deep learning,” in *Malware Analysis Using Artificial Intelligence and Deep Learning*, Springer International Publishing, 2020, pp. 581–604, doi: 10.1007/978-3-030-62582-5_23.

BIOGRAPHIES OF AUTHORS






Sheeba Thankappan Mercy    holds a Ph.D. from SRM Institute of Science and Technology, Kattankulathur, Chennai, Tamil Nadu, India. She is currently working as assistant professor in the Department of Computer Applications, Faculty of Science and Humanities, SRM Institute of Science and Technology, Kattankulathur, Chennai, Tamil Nadu, India. She has a total teaching experience of 11 years and her area of research is image processing and machine learning. She has completed Master of Computer Applications in 2003 and Master of Philosophy in 2006 from Manonmaniam Sundaranar University, Tirunelveli, Tamil Nadu, India. She has registered Ph.D. in the year 2021 in SRM Institute of Science and Technology. She can be contacted at email: st3121@srmist.edu.in.






Albert Antony Raj Saminathan    holds a Ph.D. from Manonmaniam Sundaranar University, Tirunelveli, Tamil Nadu, India. He is currently working as a professor in the Department of Computer Applications, Faculty of Science and Humanities, SRM Institute of Science and Technology, Kattankulathur, Chennai, Tamil Nadu, India. His research interest includes computer algorithms, data science, image processing and artificial intelligence. He has more than 25 years of teaching experience. He has several journal publications and is presently working on many more papers. He can be contacted at email: alberts@srmist.edu.in.



Anand Murugadhas    holds a Ph.D. from Bharathiar University, Coimbatore, Tamilnadu, India. He is currently working as an assistant professor (senior grade) in the Department of Networking and Communications, Faculty of Engineering and Technology, SRM Institute of Science and Technology, Kattankulathur, Chennai, Tamil Nadu, India. His research interest includes image processing, artificial neural networks and machine learning. He has more than 21 years in the field of teaching, he has several journal publications and is presently working on many more papers. He can be contacted at email: anandm3@srmist.edu.in.



Anshy Princella Anand Sheeba    holds a B.E. from Anna University, Chennai, Tamil Nadu, India. She is currently studying master of technology (M.Tech.) in embedded system and technology at SRM Institute of Science and Technology, Kattankulathur, Chennai, Tamil Nadu, India. She is interested in medical image processing, artificial neural networks, embedded system and machine learning. She can be contacted at email: aa6104@srmist.edu.in.